Title: ATP disrupts lipid binding equilibrium to drive retrograde transport critical for bacterial outer membrane asymmetry

Authors: Wen-Yi Low[a], Shuhua Thong[a], Shu-Sin Chng[a,b,*]

Affiliations:

[a] Department of Chemistry, National University of Singapore, Singapore 117543.

[b] Singapore Center for Environmental Life Sciences Engineering, National University of Singapore (SCELSE-NUS), Singapore 117456.

* To whom correspondence should be addressed. Email: chmchngs@nus.edu.sg

Author Contributions: W.-Y. L., S.T. and S.-S.C. designed research; W.-Y. L. performed research related to the lipid transfer assay; S.T. performed research related to the enzyme-coupled ATPase assay; W.-Y. L., S.T. and S.-S.C. analyzed data; W.-Y. L. and S.-S.C. wrote the paper.

Competing Interest Statement: The authors declare that no competing interests exist.

Classification: Biological Sciences (Biochemistry)

Keywords: outer membrane biogenesis; phospholipid transport; in vitro reconstitution; ABC transporter; MCE domain.

This PDF file includes:

Main Text

Figures 1 to 6

Abstract

The hallmark of the Gram-negative bacterial envelope is the presence of the outer membrane (OM). The OM is asymmetric, comprising lipopolysaccharides (LPS) in the outer leaflet and phospholipids (PLs) in the inner leaflet; this critical feature confers permeability barrier function against external insults, including antibiotics. To maintain OM lipid asymmetry, the OmpC-Mla system is believed to remove aberrantly localized PLs from the OM and transport them to the inner membrane (IM). Key to the system in driving lipid trafficking is the MlaFEDB ABC transporter complex in the IM, but mechanistic details, including transport directionality, remain enigmatic. Here, we develop a sensitive point-to-point in vitro lipid transfer assay that allows direct tracking of [^{14}C]-labelled PLs between the periplasmic chaperone MlaC and MlaFEDB reconstituted into nanodiscs. We reveal that MlaC spontaneously transfers PLs to the IM transporter in an MlaD-dependent manner that can be further enhanced by coupled ATP hydrolysis. In addition, we show that MlaD is important for modulating productive coupling between ATP hydrolysis and such retrograde PL transfer. We further demonstrate that spontaneous PL transfer also occurs from MlaFEDB to MlaC, but such anterograde movement is instead abolished by ATP hydrolysis. Our work uncovers a model where PLs reversibly partition between two lipid binding sites in MlaC and MlaFEDB, and ATP binding and/or hydrolysis shift this equilibrium to ultimately drive retrograde PL transport by the OmpC-Mla system. These mechanistic insights will inform future efforts towards discovering new antibiotics against Gram-negative pathogens.

42 **Significance Statement**

43 Biological membranes define cellular boundaries, allow compartmentalization, and represent a prerequisite
44 for life. In Gram-negative bacteria, the outer membrane (OM) prevents entry of toxic substances, conferring intrinsic
45 resistance against many antibiotics. This barrier function requires unequal distribution of lipids across the OM bilayer,
46 yet how such lipid asymmetry is maintained is not well understood. In this study, we established the directionality of
47 lipid transport for a conserved membrane protein complex, and uncovered mechanistic insights into how ATP powers
48 such transport from the OM to the inner membrane. Our work provides fundamental understanding of lipid trafficking
49 within the Gram-negative double-membrane envelope in the context of OM lipid asymmetry, and highlights the
50 importance of targeting lipid transport processes for future antibiotics development.

Introduction

The cell envelope of Gram-negative bacteria is composed of two lipid bilayers. The inner membrane (IM) is a phospholipid (PL) bilayer while the outer membrane (OM) contains both PLs and lipopolysaccharides (LPS). The OM is asymmetric with LPS residing in the outer leaflet and PLs in the inner leaflet; such lipid asymmetry allows the membrane to function as an effective barrier against the entry of toxic substances, including antibiotics (1, 2). Extensive efforts have contributed towards an improved understanding of the molecular mechanisms involved in OM assembly and homeostasis. We now know that the Lol, Bam, and Lpt pathways are responsible for the unidirectional transport and/or assembly of OM lipoproteins, β-barrel proteins and LPS, respectively (3-5). However, mechanisms for PL transport (6), which occur in both directions for assembly and homeostasis of the OM (7-9), remain largely elusive.

The first pathway implicated in bacterial PL transport is the OmpC-Mla system (10, 11). Cells lacking this pathway accumulate PLs in the outer leaflet of the OM, indicating a role in the maintenance of OM lipid asymmetry. The OmpC-Mla system is believed to mediate retrograde PL transport where the periplasmic MlaC chaperone shuttles PLs from the OmpC-MlaA complex in the OM to the MlaFEDB ATP-binding cassette (ABC) transporter in the IM. MlaA is an OM lipoprotein that interacts and works with trimeric osmoporin OmpC (11, 12), but forms a separate hydrophilic channel in the OM for trans-bilayer PL translocation (12, 13). While MlaA also interacts with OmpF, only removing OmpC, but not OmpF, results in OM lipid asymmetry defects in cells (11); therefore, OmpC is functionally important in the Mla system, but its exact role is unclear. MlaC is found to bind PLs with high affinity in a deep hydrophobic pocket (14-16), presumably enabling extraction of PLs from the OM via OmpC-MlaA. In the IM ABC transporter, MlaE and MlaF constitute the permease and nucleotide binding domains, respectively. MlaD is a substrate-binding protein containing a single transmembrane helix, and its periplasmic MCE domain (17) forms a hexamer with a hydrophobic pore and co-purifies with PLs (14, 18). Recent structural studies of the MlaFEDB complex revealed that the MlaE permease domains complement the MlaD hydrophobic pore to form a contiguous cavity for binding and transporting PLs (19-23). MlaB is a cytoplasmic protein containing the STAS domain (24), and has been shown to be essential for the proper assembly and activity of the IM complex (18, 25). How ATP hydrolysis may drive PL movement within the MlaFEDB complex is not known.

77 Apart from the lack of mechanistic details, there is still substantial controversy with regards to the
78 directionality of lipid transport mediated by the OmpC-Mla system. Genetic studies in *Escherichia coli* and
79 *Acinetobacter baumannii* are more consistent with the retrograde (OM-to-IM) model (10, 26). In particular, *E. coli mla*
80 or *ompC* mutants accumulate outer leaflet PLs in the OM, a phenotype that can be corrected by overexpression of
81 PldA, the OM phospholipase (10, 11). In addition, *A. baumannii* strains lacking lipooligosaccharides (LOS) have
82 enhanced growth and restored OM barrier function when the Mla system and PldA are removed, presumably because
83 these cells need enough PLs to maintain the outer leaflet of the OM (26, 27). Nevertheless, these experiments in
84 cells lack evidence that demonstrate the direct transport of PLs. While there was a report suggesting the system in
85 *A. baumannii* may be involved in anterograde (IM-to-OM) PL transport (28), it has recently been shown that the *mla*
86 mutant strains used had secondary mutations in them, thus rendering the claim invalid (29). A key experiment that
87 sheds light on transport is when the overexpression of MlaFEDB together with MlaC partially rescued defects in
88 retrograde transport of PLs, observed in *E. coli* strains lacking the Tol-Pal complex (30). Despite this, however, in
89 vitro reconstitution demonstrated ATP-independent (anterograde) transfer of PLs from the MlaFEDB complex (in
90 liposomes) to MlaC (31). These conflicting data throw into question the biological significance of ATP hydrolysis and
91 argue for the need to provide additional in vitro evidence to truly define the directionality of lipid transport mediated
92 by the OmpC-Mla system.
93 In this study, we utilize [^{14}C]-labelled lipids to directly track the point-to-point transfer of PLs between MlaC
94 and nanodisc-reconstituted MlaFEDB complex. We show that PLs bound to MlaC can be spontaneously transferred
95 to MlaFEDB in an MlaD-dependent manner. The presence of ATP further enhances such retrograde transfer; we
96 demonstrate that ATP hydrolysis is coupled to PL transport, and this process too is modulated by MlaD. Interestingly,
97 spontaneous PL transfer can also happen from MlaFEDB to MlaC, but ATP hydrolysis prevents this 'anterograde'
98 transfer, ultimately driving PL transport in the retrograde direction. Our work establishes that the OmpC-Mla system
99 powers the retrograde transport of PLs via ATP hydrolysis to maintain OM lipid asymmetry.
100

Results

MlaD stimulates the ATP hydrolytic activity of MlaFEB in a native lipid environment

To gain insights into the directionality of PL transport mediated by the OmpC-Mla system, we focused on lipid transfer between MlaC and the MlaFEDB complex embedded in a lipid bilayer. We first reconstituted MlaFEDB and MlaFEB complexes into lipid nanodiscs comprising *E. coli* polar lipids stabilized by the membrane scaffold protein MSP1E3D1 (Figure 1A) (32), and tested their functionality in ATP hydrolysis. At room temperature, the ATPase activity of nanodisc-embedded MlaFEDB was significantly lower compared to that of the same complex solubilized in detergent micelles (Figure S1A, k_{cat}: 0.029 ± 0.002 vs 0.126 ± 0.008 μmol ATP s^{-1}/μmol complex, respectively), likely due to higher conformational restriction within the membrane. This effect is similar to that observed in MlaFEDB-containing proteoliposomes composed also of native *E. coli* polar lipids (31), but opposite in complexes reconstituted in nanodiscs (21) or proteoliposomes (20) comprising synthetic lipids, suggesting an influence of lipid composition on ATPase function. At physiological temperature (37°C), however, ATP hydrolytic activity was largely recovered in the nanodisc-embedded MlaFEDB complex (k_{cat}: 0.090 ± 0.002 μmol ATP s^{-1}/μmol complex). In contrast to complexes in detergent micelles (18), we further showed that the ATPase activity of nanodisc-embedded MlaFEDB was much higher than that of MlaFEB (k_{cat}: 0.011 ± 0.002 μmol ATP s^{-1}/μmol complex) at 37°C (Figure 1B). In addition, this activity remained unaffected upon addition of holo- (PL-bound) or apo- (PL-free) MlaC (Figure S1B). The MlaFEB structure does not change significantly in the absence of MlaD (22); therefore, the presence of MlaD actually stimulates the ATP hydrolytic function of MlaFEB, consistent with MlaD being the substrate binding protein in direct contact with the ABC transporter.

MlaC transfers PLs to MlaFEDB in spontaneous and ATP-enhanced manners in vitro

We next tested the possibility of retrograde transport and investigated whether nanodisc-embedded MlaFEDB is able to extract and receive PLs from MlaC at 37°C. We incubated tag-less MlaC bound to [^{14}C]-labelled PLs (Figure S2A and S2B) with His-tagged MlaFEDB complex in non-labelled nanodiscs in a 5:1 ratio, and monitored transfer of radioactive lipids following optimal nickel affinity-based separation of the two components (Figure 2A and S2C). The nanodisc-embedded MlaFEB complex lacking MlaD was used as control; with or without ATP, a small amount of radioactive PLs on MlaC was transferred to the MlaFEB nanodiscs and treated as 'non-specific'

128 background (~11%) (Figure 2B). Interestingly, we observed a substantial increase in spontaneous transfer of
129 radioactive PLs from MlaC to nanodiscs when MlaD was present in the complex (~28% with background subtracted)
130 (Figure 2B). Following activation with ATP, even more PLs were transferred to the MlaFEDB complex (~41% with
131 background subtracted; ~1.5 fold above the level without ATP) (Figure 2C). Importantly, both the spontaneous and
132 ATP-enhanced gains in radioactive PLs on the nanodiscs were accompanied by corresponding losses from MlaC
133 (albeit with ~10-15% radioactivity unrecovered), overall indicating point-to-point PL transfer (Figure 2B). Of note, we
134 observed reduced levels of PL transfer to MlaFEDB with more MlaC added (c.f. MlaC:MlaFEDB = 1:1 vs 5:1, Figure
135 S3), possibly trending towards saturation. We have therefore reconstituted specific MlaD- and ATP-dependent
136 retrograde PL transport from MlaC to the IM ABC transporter in vitro.
137
138 **ATP hydrolysis by the MlaFEDB complex is coupled to retrograde PL transport**
139 We next characterized the observed ATP-enhanced PL transfer from MlaC to nanodisc-embedded
140 MlaFEDB. Mutations in K47 in the Walker A motif of MlaF and in the conserved T52 residue in MlaB have been
141 reported to abolish ATP hydrolytic activity of the ABC transporter in detergents (18). We showed that the Walker A
142 $MlaF_{K47A}$ variant, which is unable to hydrolyze ATP in nanodiscs (Figure 3A and S4A), still allowed spontaneous PL
143 transfer from MlaC to $MlaF_{K47A}EDB$, but completely abolished ATP-enhanced transfer (Figure 3B and S4B). In
144 addition, either the use of the non-hydrolyzable ATP analog, AMP-PNP (Figure 3C and S4C), or the ATPase inhibitor,
145 vanadate (Figure 3D, S4D and S5), similarly led to the loss of ATP-activated PL transfer from MlaC to wildtype
146 MlaFEDB, establishing that ATP hydrolysis is required for this process. Consistent with this idea, complexes with the
147 $MlaB_{T52A}$ variant (18), which we now show possesses partial ATPase activity in nanodiscs (Figures 3A and S4A),
148 exhibited correspondingly lower ATP-enhanced PL transfer from MlaC (Figure 3B and S4B). We further
149 demonstrated that the amount of radioactive PLs recovered on wildtype MlaFEDB nanodiscs reached a plateau with
150 increasing concentrations of ATP (Figure 3E and S4E), establishing that ATP-activated PL transfer is saturable and
151 thus specific. In fact, the K_M for ATP in enhanced PL transfer activity (33.1 ± 22.2 μM) is comparable to that in ATPase
152 activity of the complex (70-83 μM across multiple experiments). We conclude that ATP hydrolysis is strongly coupled
153 to retrograde PL transport mediated by the IM Mla complex.
154

155 **MlaD modulates PL binding capacity and ATP hydrolytic activity of the MlaFEDB complex in retrograde PL**
156 **transfer**

157 We next went on to investigate the role of MlaD, especially given that it is required for the transfer of PLs
158 from MlaC to the MlaFEDB complex in the absence of ATP. To do that, we examined two non-functional MlaD
159 variants that have previously been reported ($MlaD_{L106N/L107N}$ and $MlaD_{\Delta141-183}$) (14). The L106N/L107N mutation is
160 found at one of the constriction points of the central hydrophobic pore of MlaD hexamers, while the Δ141-183 deletion
161 removes the C-terminal helices that form part of the pore; both are expected to affect lipid binding of the complex. In
162 addition, $MlaD_{\Delta141-183}$ forms hexamers in the complex that are no longer SDS-resistant, exhibiting lower stability than
163 those of wildtype MlaD and $MlaD_{L106N/L107N}$ (Figure S6). Indeed, we observed elevated or reduced spontaneous
164 transfer of radioactive PLs from MlaC to nanodisc-embedded $MlaFED_{L106N/L107N}B$ (~1.3-fold) or $MlaFED_{\Delta141-183}B$ (~0.7-
165 fold, compared to wildtype MlaFEDB), respectively (Figure 4A and S7A). As expected, MlaD directly modulates the
166 PL binding capacity of the MlaFEDB complex.

167 Interestingly, these MlaD mutations also affected the ATP hydrolytic activities of the corresponding
168 complexes. The $MlaFED_{L106N/L107N}B$ complex exhibited reduced ATPase activity (Figure 4B and S7B) and hence had
169 much lower ATP-enhanced PL transfer from MlaC (Figure 4A and S7A). Remarkably, the $MlaFED_{\Delta141-183}B$ variant
170 displayed much greater ATPase activity than wildtype complex (Figure 4B and S7B), yet was unable to activate
171 additional PL transfer in the presence of ATP (Figure 4A and S7A). We conclude that MlaD modulates ATPase
172 function and is essential for coupling ATP hydrolysis to PL transfer in the MlaFEDB complex.

173

174 **ATP hydrolysis prevents spontaneous transfer of PLs from MlaFEDB to MlaC**

175 We have now established that MlaC spontaneously transfers PLs to the MlaFEDB complex in a manner that
176 can be enhanced by ATP hydrolysis. However, passive transfer of PLs from MlaFEDB to MlaC has also been
177 reported (31). To address this discrepancy, we also studied PL transfer in the anterograde direction using our
178 nanodisc-reconstituted complexes. We reconstituted MlaFEDB and MlaFEB complexes into nanodiscs containing
179 [^{14}C]-labelled PLs (Figure S8), and incubated these purified nanodiscs with tag-less apo MlaC. As negative control,
180 we showed that nanodiscs embedded MlaFEB transferred no or little PLs to MlaC (presumed non-specific transfer
181 up to ~5%) (Figure 5A and 5B). In the presence of MlaD, the MlaFEDB complex spontaneously transferred ~20% of

182 radioactive PLs from the nanodiscs to MlaC, supporting the possibility of anterograde transport (Figure 5A and 5C).
183 Remarkably, however, addition of ATP entirely prevented transfer of PLs from MlaFEDB to MlaC, and this
184 phenomenon was inhibited by addition of vanadate. Therefore, even though MlaD can spontaneously transfer PLs
185 to MlaC, ATP hydrolysis by the IM complex abolishes such activity.
186
187 **Discussion**
188 In this work, we have reconstituted ATP-powered retrograde PL transport mediated by the IM ABC
189 transporter of the OmpC-Mla system, using purified components. By applying [^{14}C]-labelled lipids, we have
190 demonstrated spontaneous PL transfer from MlaC to the MlaFEDB complex, with enhanced lipid transfer occurring
191 upon ATP hydrolysis (Figure 2). We have also observed spontaneous PL transfer from MlaFEDB to MlaC but this
192 transfer is abolished in the presence of ATP (Figure 5). Therefore, we have shown that PLs equilibrate between MlaC
193 and MlaFEDB, and ATP hydrolysis drives overall transport in the retrograde direction. Interestingly, the fold of the
194 MlaE permease domains resemble that of the LptFG counterparts in the LPS exporter (19), yet the MlaFEDB complex
195 possesses lipid import function; such ABC importers with 'exporter' folds have only recently been discovered (33-
196 35).
197 Here is a mechanistic model for MlaFEDB function, integrating all available biochemical and structural
198 information (Figure 6). In the first step, PL-bound MlaC arrives at the IM, and interacts with the MlaFEDB complex
199 via the protomer interfaces of MlaD hexamers (15). This ensues the reversible partitioning of the PL molecule(s)
200 between the lipid binding pockets of MlaC and the complex, even in the absence of ATP. While MlaD hexamers
201 alone bind PLs much less strongly than MlaC (15), the MlaFEDB complex, where several structures now reveal a
202 combined lipid binding cavity formed by both MlaD and MlaE (19-23), must possess strong affinity for PLs, likely
203 comparable to MlaC. The trajectory of PL movement between the two binding sites remains to be clarified. In the
204 second step, ATP binding has been shown to induce two conformational states of the MlaFEDB complex, believed
205 to be sequential in the process (21). Initial ATP binding to MlaF appears to cause a conformational change involving
206 upward movement of MlaD away from MlaE, which likely releases the PL molecule(s) from MlaD binding to be
207 eventually bound by MlaE alone. Subsequent complete binding of ATP induces tight dimerization of MlaF, in turn
208 collapsing the MlaE lipid binding cavity (21, 23), eventually forcing bound PL molecule(s) into the membrane. Whether

209 PLs enter the outer leaflet of the IM, or get flipped across the bilayer, is not known. In the final step, ATP hydrolysis
210 resets the MlaFEDB complex, allowing it to again adopt the nucleotide-free state. ATP binding and/or hydrolysis are
211 therefore required to overcome the energy barrier conferred by tight binding of PLs within the lipid binding cavity of
212 the MlaFEDB complex, and force them into the IM. Supporting the idea that ATP is not instead needed to release
213 lipids directly from MlaC, MlaC itself is unable to activate ATPase activity of the complex (Figure S1B). This whole
214 ATP-driven process ultimately favors retrograde PL transfer from MlaC, via the MlaFEDB complex, to the IM, in
215 accordance with the Le Chatelier's principle.

216 In the context of the model, MlaD influences both the spontaneous and ATP-coupled steps of PL transfer.
217 We speculate that the conformational flexibility of MlaD hexamers plays a major role in achieving such modulation.
218 Unlike wildtype MlaD, the $MlaD_{\Delta 141\text{-}183}$ variant exists as hexamers in the complex that are not stable to SDS (Figure
219 S6), representing a "loose" form of the hexamer with greater conformational freedom. In support of this idea, the
220 soluble domain of this variant can form heptamers in vitro (14). The MlaFEDB complex with a "loose" MlaD hexamer
221 would have a more flexible lipid binding cavity, therefore incurring greater entropic costs to bind ligands. The
222 $MlaFED_{\Delta 141\text{-}183}B$ complex may thus have a lower affinity for PLs, resulting in reduced spontaneous PL transfer from
223 MlaC (Figure 4). Increased conformational flexibility may also account for the much higher ATPase activity of this
224 variant complex, possibly by facilitating conformational movements in the MlaE permease domains associated with
225 the ATP hydrolytic cycle; however, this led to uncoupling between ATP hydrolysis and PL transfer. By analogy, we
226 posit that the $MlaD_{L106N/L107N}$ variant forms "tight" hexamers in the complex, perhaps due to more hydrogen bonding
227 interactions in the central pore. Decreased conformational flexibility thereby confers an increase in affinity for
228 spontaneous PL binding and yet a reduced ATPase activity (Figure 4). Ultimately, the $MlaFED_{L106N/L107N}B$ complex
229 has much lower ATP-enhanced PL transfer from MlaC, suggesting this non-functional variant is ineffective at forcing
230 PLs out of the MlaDE cavity into the membrane, thus unable to drive overall flux of PLs from the OM to the IM.
231 Overall, we propose that the conformational flexibility in the wildtype MlaD hexamer is optimally tuned to strike a
232 balance between PL binding and ATPase activity, yet ensure productive coupling between PL transfer and ATP
233 hydrolysis. Still, MlaD mutations may also have direct impact on PL binding enthalpies and/or interactions with MlaC.
234 Further studies to test these ideas would be needed.

235 This reconstitution addresses the controversy of directionality, and establishes that ATP drives retrograde
236 PL transport mediated by the OmpC-Mla system. Our work thus validates the interpretation of OmpC-Mla function in
237 existing genetic studies (10, 11, 26, 27), and is consistent with plastid or mycobacterial homologs of the Mla IM
238 complex being characterized as lipid uptake systems (36-38). Our highly sensitive PL transfer assay demonstrates
239 point-to-point movement of native [^{14}C]-labelled PLs between MlaC and MlaFEDB, and reveals both reversible
240 spontaneous and irreversible ATP-activated steps in the process. In the midst of preparing this manuscript, Tang et
241 al. have independently developed an indirect assay using non-native fluorescent lipids, and similarly reported that
242 the Mla pathway mediates ATP-dependent retrograde PL transport in vitro (20). While our assays are necessarily
243 complementary, the direct nature of the PL transfer assay developed here, and the use of native lipids, ultimately
244 provide stronger inference about corresponding events happening in the bacterial cell. Importantly, our work has
245 additionally uncovered the existence of a spontaneous retrograde PL transfer step from MlaC to MlaFEDB, which
246 was not detected in the Tang et al. (20) or earlier studies (31). We have also observed spontaneous anterograde PL
247 transfer from MlaFEDB to MlaC; contrary to these previous studies (20, 31), however, we have demonstrated that
248 such anterograde transfer is not ATP-independent, but is abolished and prevented by ATP hydrolysis. These two
249 significant findings set us apart from the Tang et al. work, directly advancing our understanding of how ATP
250 binding/hydrolysis is coupled to PL transfer at the MlaFEDB complex to ultimately drive PL transport in the retrograde
251 fashion. Collectively, both the fluorescence-based and radioactivity-based assays establish the directionality of the
252 system. These PL transport assays will continue to serve as critical tools for detailed mechanistic studies, and for
253 future identification and validation of small molecule inhibitors against the OmpC-Mla pathway. Adapted assays can
254 also be applied to study possible lipid transport mediated by other putative systems, including the Tol-Pal complex
255 (30) and other MCE domain-containing complexes (14, 39, 40).
256

257 **Materials and Methods**

258 **Reconstitution of membrane proteins in lipid nanodiscs**

259 The reconstitutions of purified membrane proteins (MlaF(His-E)B, MlaF(His-E)DB, MlaF$_{K47A}$(His-E)DB,
260 MlaF(His-E)DB$_{T52A}$, MlaF(His-E)D$_{L106/L107N}$B and MlaF(His-E)D$_{\Delta 141-183}$B) into nanodiscs were adapted from published
261 protocols (32). 10 mg of *E. coli* polar lipid extracts (Avanti Polar Lipids) were dissolved in 1 mL of chloroform and
262 dried overnight. 1 mL of TBS buffer (20 mM Tris.HCl pH 8.0, 150 mM NaCl) containing 25 mM sodium cholate
263 (Sigma-Aldrich) was added to the dried lipid film, and vortexed and sonicated until a clear solution was obtained. The
264 respective Mla complex, the membrane scaffold protein MSP1E3D1-His and lipid were mixed at a molar ratio of
265 1:10:1500 in TBS and incubated, with rocking, for 1 h at 4 °C. Bio-beads SM2 resin (Bio-Rad) was subsequently
266 added to the solution (30 mg per 1-mL reconstitution mixture) and incubated with gentle agitation for 3 h at 4 °C.
267 Upon removal of Bio-beads, the sample was concentrated and purified by size exclusion chromatography (SEC) on
268 a Superose 6 Increase 10/300 GL column (GE Healthcare) on ÄKTA™ Pure. 0.5-mL fractions were collected and
269 subjected to SDS-PAGE analysis and Coomassie blue staining (InstantBlue™, expedeon). Fractions containing the
270 nanodisc-embedded complex were pooled and concentrated on a 30 kDa cut-off ultra-filtration device (Amicon Ultra,
271 Merck Millipore). For the reconstitution of radioactive nanodisc-embedded MlaF(His-E)B and MlaF(His-E)DB
272 complexes, [^{14}C]-labelled PLs extracted from [^{14}C]-acetate labelled cells were used in place of *E. coli* polar lipid
273 extracts, and the nanodiscs samples were purified on a self-packed column containing Superose 6 Prep Grade (GE
274 Healthcare) instead.

275

276 **In vitro PL transfer assays**

277 For in vitro retrograde PL transfer experiments, 10 μM of purified tag-less MlaC bound to [^{14}C]-labelled PLs
278 was incubated with 2 μM of purified non-radioactive His-tagged nanodisc-embedded complex. For in vitro
279 anterograde PL transfer experiments, 10 μM of purified tag-less apo MlaC was incubated with 2 μM of purified His-
280 tagged nanodisc-embedded complex reconstituted with [^{14}C]-labelled PLs. These components were incubated in 400
281 μL TBS buffer, either in the absence or presence of 2 mM ATP (Sigma-Aldrich) and 2 mM $MgCl_2$, for 10 min at 37°C.
282 After the transfer reaction, the mixture was topped up with TBS to a final volume of 2.5 mL, and incubated with 0.5
283 mL nickel resin (His60 Ni Superflow Resin, Takara Bio) in a Poly-Prep chromatography column (BioRad) for 1h, with

284 rocking, at room temperature. The filtrate (containing separated tag-less MlaC) was collected after the mixture was
285 passed through the resin twice. The resin was washed with 5 x 4 mL TBS containing 30 mM imidazole, and the
286 nanodisc-embedded complex was eluted with 2.5 mL TBS containing 300 mM imidazole. Samples obtained from the
287 nickel affinity-based separation were subjected to SDS-PAGE analysis and visualized by silver staining to ensure
288 that there was minimal cross-contamination of the two components. For experiments involving vanadate, 2 μM of the
289 nanodisc-embedded MlaFEDB complex was first pre-incubated with 2 mM ATP and 2 mM $MgCl_2$ for 5 min, then with
290 2.7 mM vanadate for 10 min, before finally incubating with 10 μM of MlaC for 10 min for PL transfer. 2 mM AMP-PNP
291 (Sigma-Aldrich) was also used in place of ATP for specific transfer experiments. All transfer experiments were
292 conducted in triplicates.

293 After separation of the filtrate (tag-less MlaC) and eluate (His-tagged nanodisc-embedded complex), 2 mL
294 of each component was added to 2 mL Ultima Gold scintillation fluid (PerkinElmer), and radioactivity counted on the
295 MicroBeta2 scintillation counter (PerkinElmer). The recovery of tag-less MlaC was quantified using the ratio standard
296 curve method (41) while that of His-tagged nanodisc-embedded complexes were quantified using the Lowry assay
297 (DC Protein Assay, Bio-Rad). For retrograde assay, the average gains and losses of radioactivity in the nanodiscs
298 and MlaC, respectively, were normalized to the initial [14C]-counts in MlaC using the following equation:

299 $$\text{Recovered radioactivity} = \frac{[14\text{C}]\text{ counts associated with sample}}{\frac{\text{Amount of sample recovered}}{\text{Initial amount of sample used}}} \times \frac{100\%}{\text{Initial count on MlaC}}$$

300 Fold changes in gains and losses of radioactivity in the nanodiscs and MlaC, respectively, were derived after
301 accounting for MlaFEB background and normalized to data from co-incubation of MlaFEDB/MlaC without ATP
302 (MlaFEDB (-ATP)). The starting radioactivity on [^{14}C]-PL-bound MlaC were in the range of 12790-22854 cpm (or
303 13606-24313 dpm).

304 For the anterograde assay, the average gains and losses of radioactivity in the MlaC and nanodiscs,
305 respectively, were normalized to the initial [14C]-counts in nanodisc using the following equation:

306 $$\text{Recovered radioactivity} = \frac{[14\text{C}]\text{ counts associated with sample}}{\frac{\text{Amount of sample recovered}}{\text{Initial amount of sample used}}} \times \frac{100\%}{\text{Initial count on nanodisc}}$$

307 The starting radioactivity on nanodiscs containing [^{14}C]-PLs were in the range of 75485-95725 cpm (or 80303-101835
308 dpm).

Acknowledgments

W.-Y.L. was supported by the National University of Singapore President's Graduate Fellowship (PGF). This work was supported by the Singapore Ministry of Health National Medical Research Council under its Open Fund Individual Research Grant (MOH-000145) (to S.-S.C.). The authors declare no conflict of interest.

References

1. Y. Kamio, H. Nikaido, Outer membrane of *Salmonella typhimurium*: accessibility of phospholipid head groups to phospholipase C and cyanogen bromide activated dextran in the external medium. *Biochemistry* 15, 2561-2570 (1976).
2. H. Nikaido, Molecular basis of bacterial outer membrane permeability revisited. *Microbiol. Mol. Biol. Rev.* 67, 593-656 (2003).
3. S. Okuda, H. Tokuda, Lipoprotein sorting in bacteria. *Annu. Rev. Microbiol.* 65, 239-259 (2011).
4. P. Sperandeo, A. M. Martorana, A. Polissi, Lipopolysaccharide biogenesis and transport at the outer membrane of Gram-negative bacteria. *Biochim. Biophys. Acta.* 1862, 1451-1460 (2017).
5. N. Noinaj, J. C. Gumbart, S. K. Buchanan, The beta-barrel assembly machinery in motion. *Nat. Rev. Microbiol.* 15, 197-204 (2017).
6. R. Shrivastava, S.-S. Chng, Lipid trafficking across the Gram-negative cell envelope. *J. Biol. Chem.* 294, 14175-14184 (2019).
7. A. M. Donohue-Rolfe, M. Schaechter, Translocation of phospholipids from the inner to the outer membrane of *Escherichia coli*. *Proc. Natl. Acad. Sci. U.S.A.* 77, 1867-1871 (1980).
8. N. C. Jones, M. J. Osborn, Translocation of phospholipids between the outer and inner membranes of *Salmonella typhimurium*. *J Biol Chem* 252, 7405-7412 (1977).
9. K.E. Langley, E. Hawrot, E.P. Kennedy, Membrane assembly: movement of phosphatidylserine between the cytoplasmic and outer membranes of *Escherichia coli*. *J. Bacteriol.* 152, 1033–1041 (1982).
10. J. C. Malinverni, T. J. Silhavy, An ABC transport system that maintains lipid asymmetry in the Gram-negative outer membrane. *Proc. Natl. Acad. Sci. U.S.A.* 106, 8009-8014 (2009).

335 11. Z.-S. Chong, W.-F. Woo, S.-S. Chng, Osmoporin OmpC forms a complex with MlaA to maintain outer
336 membrane lipid asymmetry in *Escherichia coli*. *Mol. Microbiol.* 98, 1133-1146 (2015).
337 12. J. Yeow *et al.*, The architecture of the OmpC-MlaA complex sheds light on the maintenance of outer
338 membrane lipid asymmetry in *Escherichia coli*. *J. Biol. Chem.* 293, 11325-11340 (2018).
339 13. J. Abellon-Ruiz *et al.*, Structural basis for maintenance of bacterial outer membrane lipid asymmetry. *Nat.*
340 *Microbiol.* 2, 1616-1623 (2017).
341 14. D. C. Ekiert *et al.*, Architectures of lipid transport systems for the bacterial outer membrane. *Cell* 169, 273-
342 285 e217 (2017).
343 15. B. Ercan, W.-Y. Low, X. Liu, S.-S. Chng, Characterization of interactions and phospholipid transfer between
344 substrate binding proteins of the OmpC-Mla system. *Biochemistry* 58, 114-119 (2019).
345 16. D. Yero *et al.*, The *Pseudomonas aeruginosa* substrate-binding protein Ttg2D functions as a general
346 glycerophospholipid transporter across the periplasm. *Commun. Biol.* 4, 448 (2021).
347 17. G. L. Isom *et al.*, MCE domain proteins: conserved inner membrane lipid-binding proteins required for outer
348 membrane homeostasis. *Sci. Rep.* 7, 8608 (2017).
349 18. S. Thong *et al.*, Defining key roles for auxiliary proteins in an ABC transporter that maintains bacterial outer
350 membrane lipid asymmetry. *eLife* 5, e19042 (2016).
351 19. N. Coudray *et al.*, Structure of bacterial phospholipid transporter MlaFEDB with substrate bound. *eLife* 9,
352 e62518 (2020).
353 20. X. Tang *et al.*, Structural insights into outer membrane asymmetry maintenance in Gram-negative bacteria
354 by MlaFEDB. *Nat. Struct. Mol. Biol.* 28, 81-91 (2021).
355 21. X. Chi *et al.*, Structural mechanism of phospholipids translocation by MlaFEDB complex. *Cell Res.* 30, 1127-
356 1135 (2020).
357 22. C. Zhou *et al.*, Structural Insight into Phospholipid Transport by the MlaFEBD Complex from *P. aeruginosa*.
358 *J. Mol. Biol.* 433, 166986 (2021).
359 23. Y. Zhang, Q. Fan, X. Chi, Q. Zhou, Y. Li, Cryo-EM structures of *Acinetobacter baumannii* glycerophospholipid
360 transporter. *Cell Discov.* 6, 86 (2020).

361 24. L. Aravind, E.V. Koonin, The STAS domain - a link between anion transporters and antisigma-factor
362 antagonists. *Curr. Biol.* 10, R53–R55 (2000).
363 25. L. R. Kolich *et al.*, Structure of MlaFB uncovers novel mechanisms of ABC transporter regulation. *eLife* 9,
364 e60030 (2020).
365 26. M. J. Powers, M. S. Trent, Phospholipid retention in the absence of asymmetry strengthens the outer
366 membrane permeability barrier to last-resort antibiotics. *Proc. Natl. Acad. Sci. U.S.A.* 115, E8518-E8527
367 (2018).
368 27. E. Nagy, R. Losick, D. Kahne, Robust suppression of lipopolysaccharide deficiency in *Acinetobacter*
369 *baumannii* by growth in minimal medium**.** *J. Bacteriol.* 201, e00420-19 (2020).
370 28. C. Kamischke *et al.*, The *Acinetobacter baumannii* Mla system and glycerophospholipid transport to the outer
371 membrane. *eLife* 8, e40171 (2019).
372 29. M. J. Powers, B. W. Simpson, M. S. Trent, The Mla pathway in *Acinetobacter baumannii* has no
373 demonstrable role in anterograde lipid transport. *eLife* 9, e56571 (2020).
374 30. R. Shrivastava, X. Jiang, S.-S. Chng, Outer membrane lipid homeostasis via retrograde phospholipid
375 transport in *Escherichia coli*. *Mol. Microbiol.* 106, 395-408 (2017).
376 31. G. W. Hughes *et al.*, Evidence for phospholipid export from the bacterial inner membrane by the Mla ABC
377 transport system. *Nat. Microbiol.* 4, 1692-1705 (2019).
378 32. T. K. Ritchie *et al.*, Reconstitution of membrane proteins in phospholipid bilayer nanodiscs. *Methods*
379 *enzymo*l. 464, 211-231 (2009).
380 33. Z. Wang, W. Hu, H. Zheng, Pathogenic siderophore ABC importer YbtPQ adopts a surprising fold of exporter.
381 *Sci. Adv.* 6, eaay7997 (2020).
382 34. F. M. Arnold *et al.*, The ABC exporter IrtAB imports and reduces mycobacterial siderophores. *Nature* 580,
383 413-417 (2020).
384 35. S. Rempel *et al.*, A mycobacterial ABC transporter mediates the uptake of hydrophilic compounds. *Nature*
385 580, 409-412 (2020).
386 36. C. Benning, Mechanisms of lipid transport involved in organelle biogenesis in plant cells. *Annu. Rev. Cell*
387 *Dev. Biol.* 25, 71-91 (2009).

388 37. A. K. Pandey, C. M. Sassetti, Mycobacterial persistence requires the utilization of host cholesterol. *Proc.*
389 *Natl. Acad. Sci. U.S.A.* 105, 4376-4380 (2008).
390 38. S. A. Cantrell *et al.*, Free mycolic acid accumulation in the cell wall of the mce1 operon mutant strain of
391 *Mycobacterium tuberculosis*. *J. Microbiol.* 51, 619-626 (2013).
392 39. G. L. Isom *et al.*, LetB structure reveals a tunnel for lipid transport across the bacterial envelope. *Cell* 181,
393 653-664 e619 (2020)
394 40. C. Liu, J. Ma, J. Wang, H. Wang, L. Zhang, Cryo-EM structure of a bacterial lipid transporter YebT. *J. Mol.*
395 *Biol.* 432, 1008-1019 (2020).
396 41. A. Pitre, Y. Pan, S. Pruett, O. Skalli, On the use of ratio standard curves to accurately quantitate relative
397 changes in protein levels by western blot. *Anal. Biochem.* 361, 305-307 (2007).

398 **Figures**

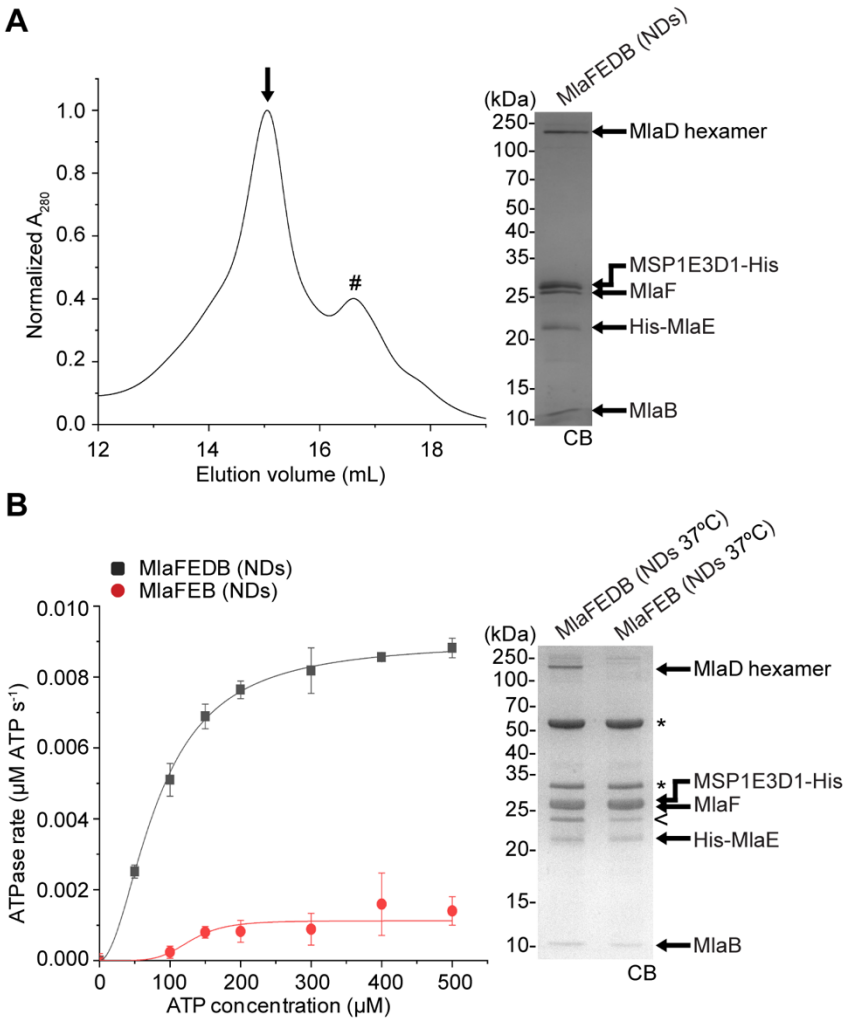

399

400 **Figure 1.** Nanodisc-embedded MlaFEDB exhibits higher ATP hydrolytic activity than MlaFEB. (A) Size-exclusion
401 chromatographic profile of nanodisc-reconstituted (NDs) MlaFEDB complex. SDS-PAGE analysis of the peak fraction
402 (annotated with an arrow (↓)) is shown on the right. #, empty NDs. (B) Enzyme-coupled ATPase assays of nanodisc-
403 embedded MlaFEDB and MlaFEB complexes (0.1 μM) at 37°C. Average ATP hydrolysis rates from triplicate
404 experiments were plotted against ATP concentrations, and fitted to an expanded Michaelis-Menten equation that
405 includes a term for Hill coefficient (n); MlaFEDB NDs (k_{cat} = Vmax/[complex] = 0.090 ± 0.002 μmol ATP s^{-1}/μmol
406 complex, K_m = 82.5 ± 4.3 μM, n = 1.9 ± 0.2) and MlaFEB NDs (k_{cat} = 0.011 ± 0.002 μmol ATP s^{-1}/μmol complex, K_m
407 = 129.1 ± 12.8 μM, n = 5.3 ± 2.0). Errors depicted by bars and ± signs are standard deviations of triplicate data. SDS-

408 PAGE analysis of the complexes used for these assays is shown on the right. *, pyruvate kinase/lactate
409 dehydrogenase enzymes used in coupled assay; <, degraded MSP1E3D1. CB, Coomassie blue staining.
410

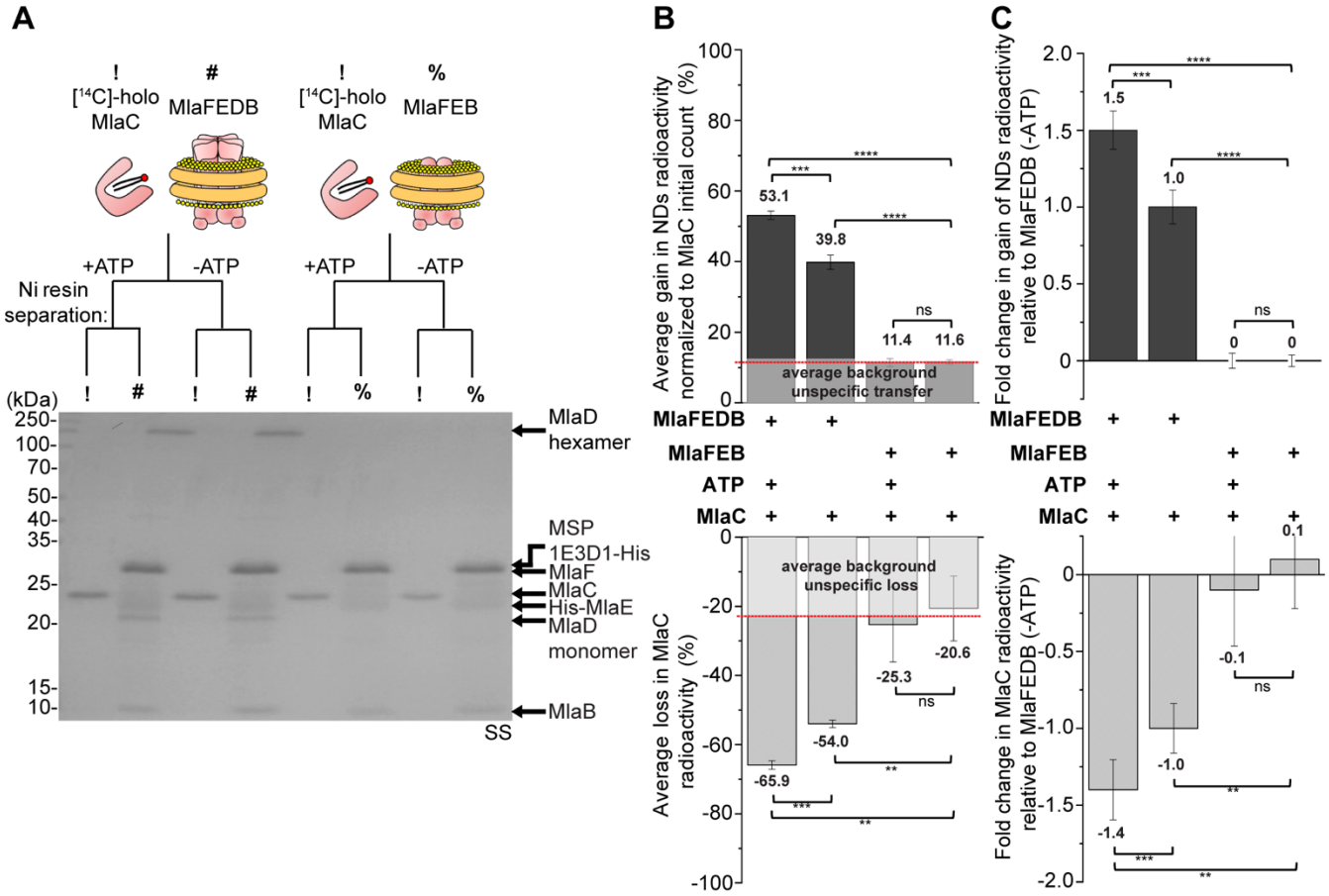

Figure 2. MlaC transfers [^{14}C]-labelled lipids to nanodisc-embedded MlaFEDB in an MlaD- and ATP-dependent manner. (A) SDS-PAGE analysis of indicated samples following co-incubation with or without ATP, and subsequent nickel affinity-based clean separation of tag-less [^{14}C]-PL bound (holo) MlaC (10 μM) and His-tagged non-radioactive nanodisc-embedded complexes (2 μM). !, [^{14}C]-holo MlaC; #, nanodisc-embedded MlaFEDB; %, nanodisc-embedded MlaFEB; SS, silver staining. (B) Average gains and losses of radioactivity ([^{14}C]-lipids) in the indicated nanodiscs (*top*) and MlaC (*bottom*), respectively, normalized to the initial counts on MlaC. Data from co-incubation of MlaFEB/MlaC are treated as unspecific background transfer/loss. (C) Fold changes in gains and losses of radioactivity in the indicated nanodiscs (*top*) and MlaC (*bottom*), respectively, derived from (B) after accounting for MlaFEB background and normalized to data from co-incubation of MlaFEDB/MlaC without ATP (MlaFEDB (-ATP)). Error bars represent standard deviations calculated from triplicate experiments. Student's t-tests: ns, not significant; **, $p < 0.01$; ***, $p < 0.001$, ****; $p < 0.0001$.

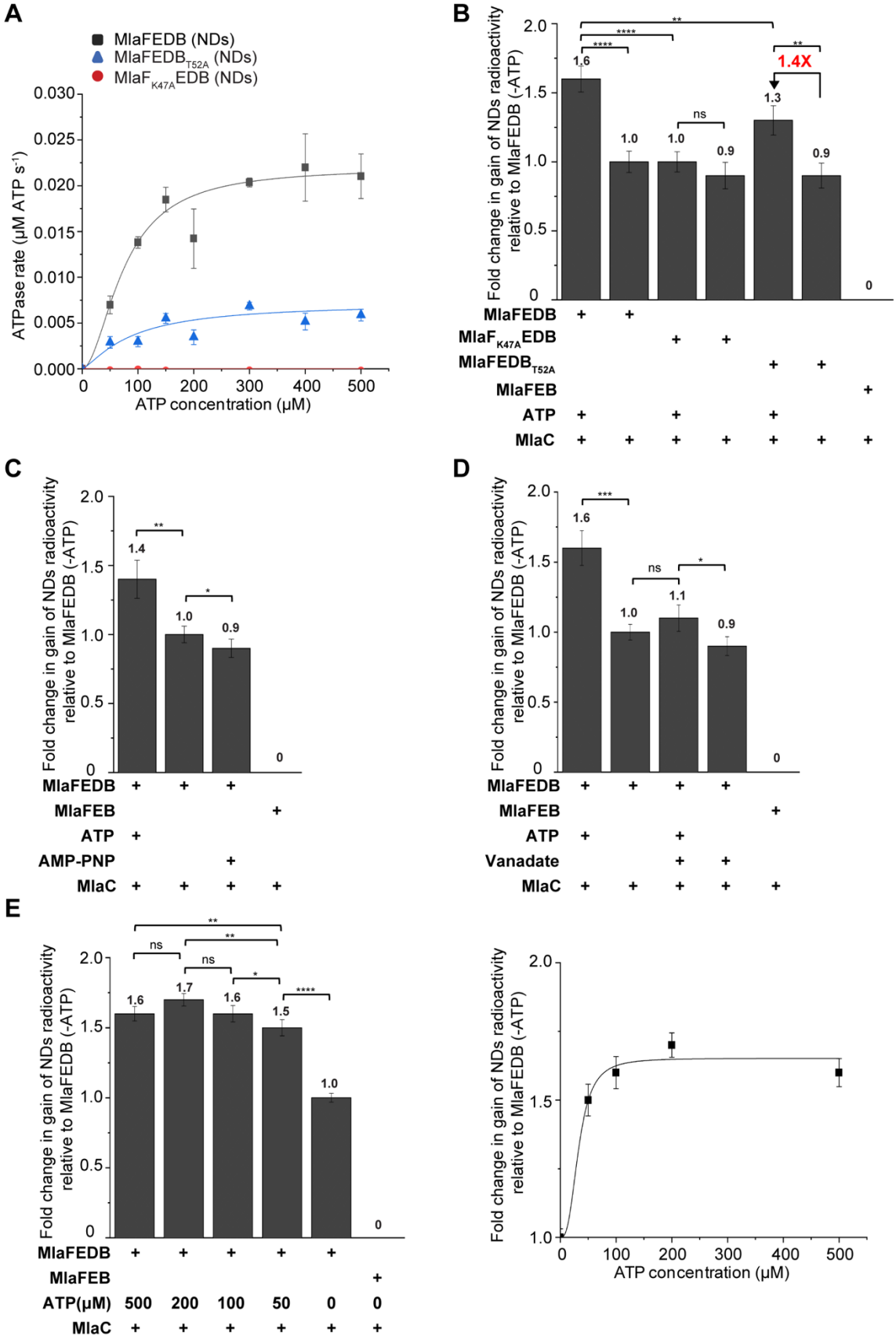
A
MlaFEDB (NDs)
MlaFEDB$_{T52A}$ (NDs)
MlaF$_{K47A}$EDB (NDs)
ATPase rate (μM ATP s^{-1})
ATP concentration (μM)
B
Fold change in gain of NDs radioactivity relative to MlaFEDB (-ATP)
1.4X
MlaFEDB
MlaF$_{K47A}$EDB
MlaFEDB$_{T52A}$
MlaFEB
ATP
MlaC
C
Fold change in gain of NDs radioactivity relative to MlaFEDB (-ATP)
MlaFEDB
MlaFEB
ATP
AMP-PNP
MlaC
D
Fold change in gain of NDs radioactivity relative to MlaFEDB (-ATP)
MlaFEDB
MlaFEB
ATP
Vanadate
MlaC
E
Fold change in gain of NDs radioactivity relative to MlaFEDB (-ATP)
MlaFEDB
MlaFEB
ATP(μM)
MlaC
Fold change in gain of NDs radioactivity relative to MlaFEDB (-ATP)
ATP concentration (μM)

424

425 **Figure 3.** ATP hydrolysis is coupled to retrograde PL transport. (A) Enzyme-coupled ATPase assays of nanodisc-
426 embedded MlaFEDB, MlaFEDB$_{T52A}$ and MlaF$_{K47A}$EDB complexes (0.1 μM) at 37°C. Average ATP hydrolysis rates
427 from triplicate experiments were plotted against ATP concentrations, and fitted to an expanded Michaelis-Menten
428 equation that includes a term for Hill coefficient (n); MlaFEDB NDs (k_{cat} = 0.220 ± 0.000 μmol ATP s^{-1}/μmol complex,
429 K_m = 75.0 ± 8.0 μM, n = 1.9 ± 0.4), MlaFEDB$_{T52A}$ NDs (k_{cat} = 0.072 ± 0.028 μmol ATP s^{-1}/μmol complex, K_m = 88.4 ±
430 62.1 μM, n = 1.3 ± 1.2). SDS-PAGE analysis of the complexes used for the assay is shown in Figure S4A. (B-E) Fold
431 changes in gains of radioactivity ([^{14}C]-lipids) in indicated nanodiscs, following co-incubation and subsequent nickel
432 affinity-based separation of tag-less [^{14}C]-PL bound (holo) MlaC (10 μM) and His-tagged non-radioactive nanodisc-
433 embedded complexes (2 μM), for (B) ATPase mutant complexes, (C) addition of AMP-PNP, (D) addition of vanadate
434 (2.7 mM), and (E) different ATP concentrations. Data from (E) are replotted on the right and fitted to an expanded
435 Michaelis-Menten equation that includes a term for Hill coefficient (n); MlaFEDB NDs (K_m for ATP during PL transfer
436 = 33.1 ± 22.2 μM, n = 2.8 ± 4.6, R^2 = 0.9891). SDS-PAGE analyses depicting clean separation of nanodisc-embedded
437 complexes and MlaC are shown in Figure S4B-E. Fold changes are derived from average gains in radioactivity counts
438 in indicated nanodiscs, after accounting for MlaFEB background and normalized to data from MlaFEDB (-ATP).
439 Errors depicted by bars and ± signs are standard deviations from triplicate data. Student's t-tests: ns, not significant;
440 *, $p < 0.05$; **, $p < 0.01$; ***, $p < 0.001$; ****, $p < 0.0001$.
441

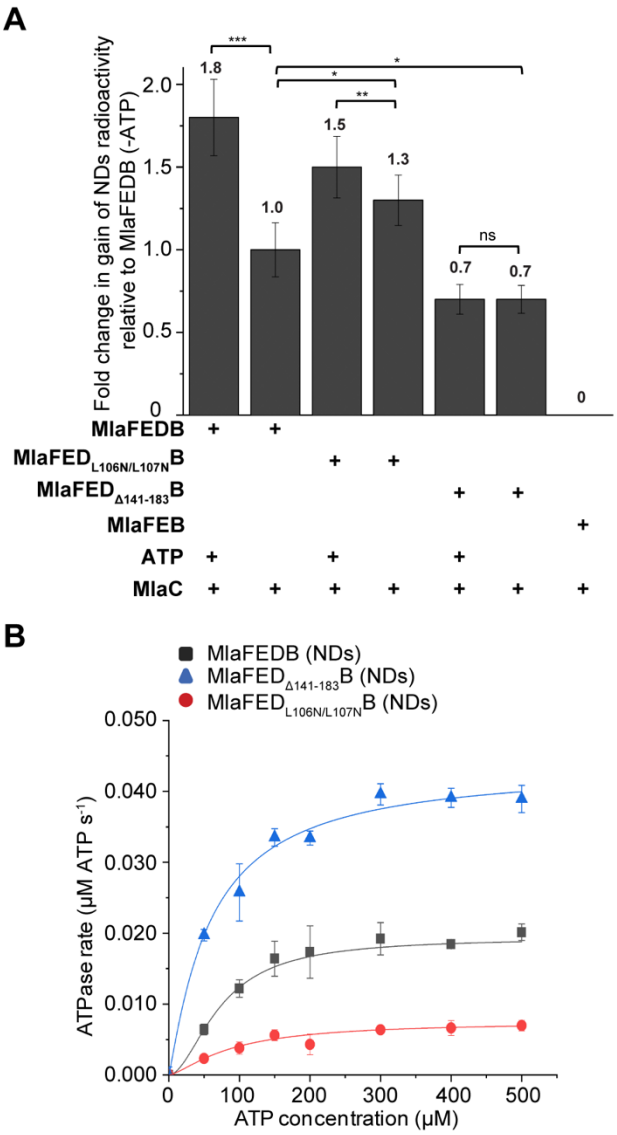

Figure 4. MlaD modulates both the spontaneous and ATP-activated PL transfer steps. (A) Fold changes in gains of radioactivity ([^{14}C]-lipids) in indicated nanodiscs, following co-incubation and subsequent nickel affinity-based separation of tag-less [^{14}C]-PL bound (holo) MlaC (10 μM) and His-tagged non-radioactive nanodisc-embedded complexes containing MlaD variants (2 μM). SDS-PAGE analyses depicting clean separation of nanodisc-embedded complexes and MlaC are shown in Figure S7A. Fold changes are derived from average gains in radioactivity counts in indicated nanodiscs, after accounting for MlaFEB background and normalized to data from MlaFEDB (-ATP). (B) Enzyme-coupled ATPase assays of nanodisc-embedded MlaFEDB, MlaFED$_{L106N/L107N}$B and MlaFED$_{\Delta141-183}$B complexes (0.1 μM) at 37°C. Average ATP hydrolysis rates from triplicate experiments were plotted against ATP

451 concentrations, and fitted to an expanded Michaelis-Menten equation that includes a term for Hill coefficient (n);
452 MlaFEDB NDs (k_{cat} = 0.193 ± 0.007 μmol ATP s^{-1}/μmol complex, K_m = 73.2 ± 6.9 μM, n = 1.8 ± 0.4),
453 MlaFED$_{L106N/L107N}$B NDs (k_{cat} = 0.075 ± 0.011 μmol ATP s^{-1}/μmol complex, K_m = 88.7 ± 26.3 μM, n = 1.4 ± 0.5) and
454 MlaFED$_{\Delta 141-183}$B NDs (k_{cat} = 0.436 ± 0.027 μmol ATP s^{-1}/μmol complex, K_m = 59.2 ± 7.5 μM, n = 1.1 ± 0.2). SDS-
455 PAGE analysis of the complexes used for the assay is shown in Figure S7B. Errors depicted by bars and ± signs are
456 standard deviations from triplicate data. Student's t-tests: ns, not significant; *, $p < 0.05$; **, $p < 0.01$; ***, $p < 0.001$.
457

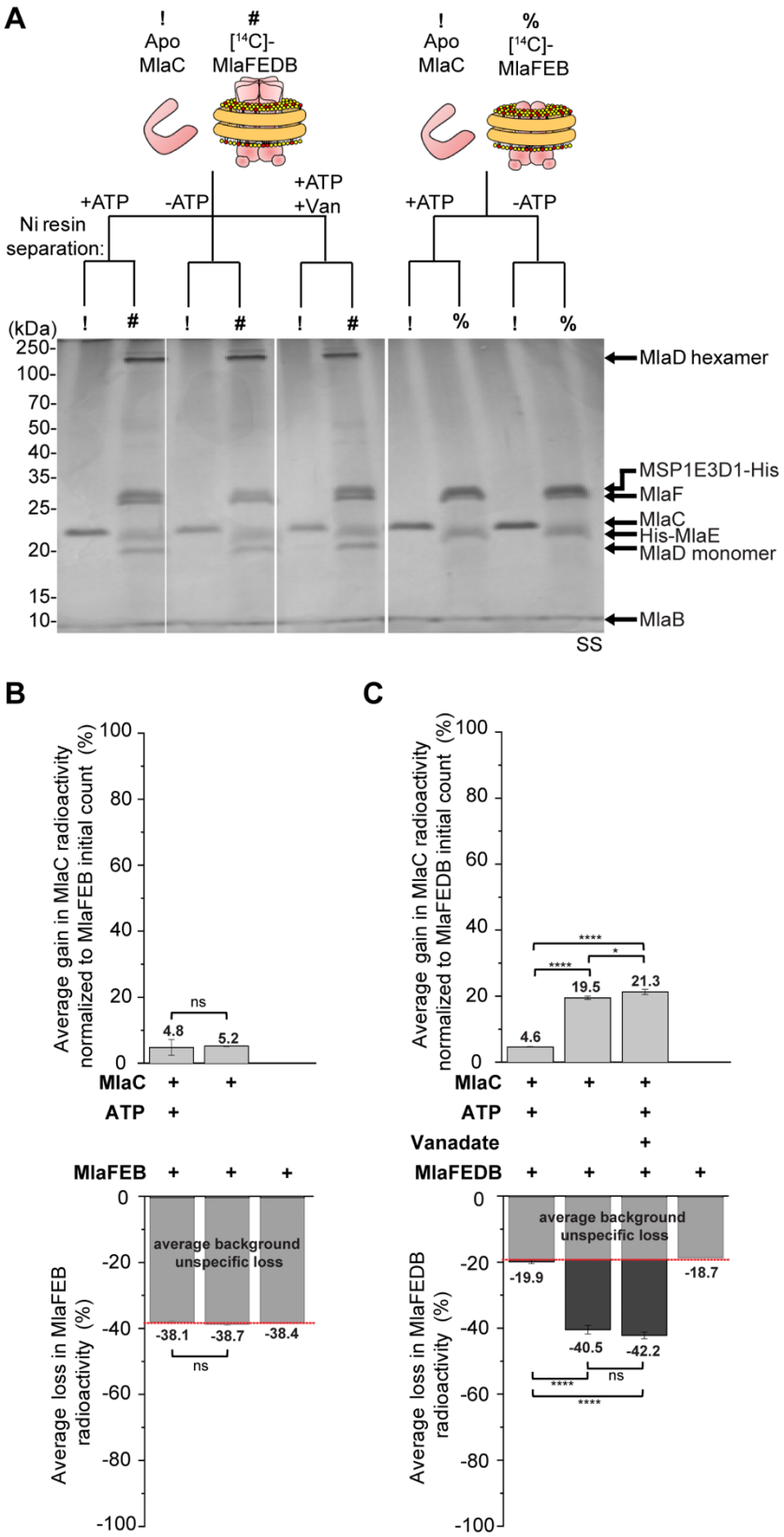
A
! Apo MlaC
[14C]-MlaFEDB
! Apo MlaC
% [14C]-MlaFEB
+ATP
-ATP
+ATP +Van
+ATP
-ATP
Ni resin separation:
(kDa)
250-
100-
70-
50-
40-
35-
25-
20-
15-
10-
MlaD hexamer
MSP1E3D1-His
MlaF
MlaC
His-MlaE
MlaD monomer
MlaB
SS
B
Average gain in MlaC radioactivity normalized to MlaFEB initial count (%)
ns
4.8
5.2
MlaC
ATP
MlaFEB
average background unspecific loss
-38.1
-38.7
-38.4
ns
Average loss in MlaFEB radioactivity (%)
C
Average gain in MlaC radioactivity normalized to MlaFEDB initial count (%)
****
*
****
4.6
19.5
21.3
MlaC
ATP
Vanadate
MlaFEDB
average background unspecific loss
-19.9
-40.5
-42.2
-18.7
****
ns
****
Average loss in MlaFEDB radioactivity (%)

458

459 **Figure 5.** ATP hydrolysis abolishes spontaneous transfer of PLs from MlaFEDB to MlaC. (A) SDS-PAGE analysis of
460 indicated samples following co-incubation with or without ATP, or vanadate, and subsequent nickel affinity-based
461 clean separation of tag-less non-radioactive apo MlaC (10 μM) and His-tagged nanodisc-embedded complexes
462 reconstituted with [^{14}C]-PLs (2 μM). !, apo MlaC; #, nanodisc-embedded [^{14}C]-MlaFEDB; %, nanodisc-embedded
463 [^{14}C]-MlaFEB; SS, silver staining. (B) Average gains and losses of radioactivity ([^{14}C]-lipids) in MlaC (*top*) and MlaFEB
464 (*bottom*), respectively, normalized to the initial counts on MlaFEB. (C) Average gains and losses of radioactivity
465 ([^{14}C]-lipids) in MlaC (*top*) and MlaFEDB (*bottom*), respectively, normalized to the initial counts on MlaFEDB. Data
466 from co-incubation of MlaFEB/MlaFEDB with nickel resin alone are treated as unspecific background loss. Error bars
467 represent standard deviations calculated from triplicate experiments. Student's t-tests: ns, not significant; *, $p < 0.05$;
468 ****; $p < 0.0001$.
469

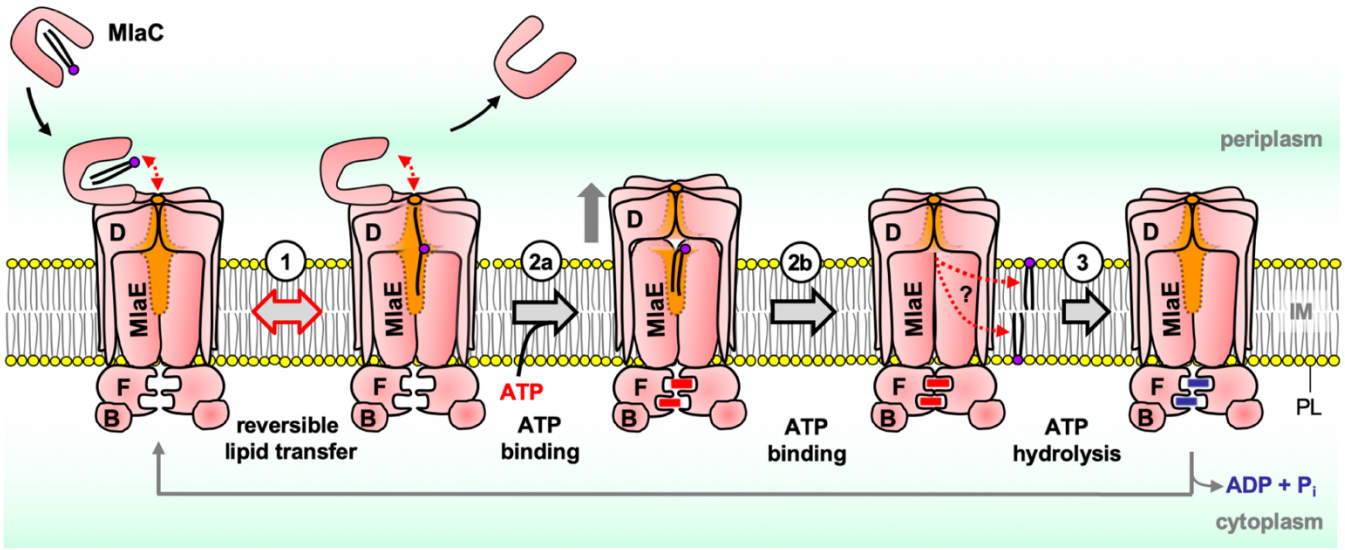

Figure 6. Proposed mechanistic model for MlaFEDB function in retrograde PL transfer. Step 1: Upon MlaC binding, reversible spontaneous transfer of PL cargo occurs between the lipid binding pocket in MlaC and the lipid binding cavity formed by both MlaD and MlaE in the complex (illustrated in orange). Step 2a: Initial ATP binding to MlaF may induce a state where MlaD moves away from MlaE (illustrated by grey arrow), possibly facilitating lipid binding by MlaE alone (21). Step 2b: Complete ATP binding eventually causes dimerization of MlaF, along with the collapse of the lipid binding cavity in MlaE, thus forcing the PL molecule into the membrane (21, 23). It is not clear which leaflet of the IM the PL molecule goes into. Step 3: Hydrolysis of ATP then resets such conformational changes, so the complex can return to the nucleotide apo state.